



ATLAS NOTE

ATLAS-CONF-2012-153

November 11, 2012



Search for Supersymmetry in events with four or more leptons in 13.0 fb^{-1} pp collisions at $\sqrt{s} = 8 \text{ TeV}$ with the ATLAS detector

The ATLAS Collaboration

Abstract

Results of a search for supersymmetry in events with four or more leptons (electrons or muons) are presented. The analysis uses a sample corresponding to 13.0 fb^{-1} of proton-proton collision data delivered by the LHC at $\sqrt{s} = 8 \text{ TeV}$ and recorded by the ATLAS detector. Two signal regions are defined with a selection vetoing Z boson production. The first signal region has large missing transverse momentum ($E_T^{\text{miss}} > 50 \text{ GeV}$), where 1 event is observed while $0.25^{+0.29}_{-0.25}$ are expected from Standard Model processes. The second requires large total effective mass ($m_{\text{eff}} > 300 \text{ GeV}$), where 2 events are observed while 1.2 ± 0.5 are expected from Standard Model processes. Limits are placed on various R-parity violating simplified models, where the lightest supersymmetric particle ($\tilde{\chi}_1^0$) decays promptly to first- and second-generation leptons. Considering one other sparticle at a time, pair-produced and decaying directly to a $\tilde{\chi}_1^0$, charged Winos are excluded up to a mass of $\sim 710 \text{ GeV}$, left-handed sleptons up to $\sim 450 \text{ GeV}$, sneutrinos up to $\sim 410 \text{ GeV}$ and gluinos up to $\sim 1300 \text{ GeV}$.

1 Introduction

Supersymmetry (SUSY) [1] is one of the most popular theoretical extensions of the Standard Model (SM). SUSY is able to stabilise the mass of the Higgs boson and unify gauge couplings through the introduction of “superpartner” fermions and bosons for each SM boson and fermion, respectively. In the most general formulation of SUSY, the proton becomes unstable due to new baryon-and lepton-number violating terms in the superpotential [2]:

$$W_{\text{RPV}} = \lambda_{ijk} L_i L_j \bar{E}_k + \lambda'_{ijk} L_i Q_j \bar{D}_k + \lambda''_{ijk} \bar{U}_i \bar{D}_j \bar{D}_k + \kappa_i L_i H_2, \quad (1)$$

where L_i and Q_i denote the lepton and quark SU(2) doublet superfields, respectively, while the corresponding singlet superfields are given by \bar{E}_i and \bar{D}_i . H_2 denotes the Higgs SU(2) doublet superfield that couples to up-like quarks. λ_{ijk} , λ'_{ijk} and λ''_{ijk} are new Yukawa couplings and the κ_i have dimensions of mass, but vanish at the unification scale. The indices i , j and k refer to quark and lepton generations.

It is often assumed in supersymmetric models that R-parity is conserved, which has the effect of forbidding the superpotential terms in Equation (1) [3]. This symmetry makes the lightest SUSY particle (LSP) stable, allowing it to be a dark matter candidate [4]. Additionally, the LSP is forbidden on cosmological grounds from carrying electric or colour charges. In a collider experiment, production of SUSY particles decaying to the LSP would produce significant amounts of missing transverse momentum (E_T^{miss}), a characteristic that drives many searches for supersymmetric particle production.

It may be, however, that the proton lifetime is protected by another, less stringent, symmetry that allows some of the terms in Equation (1). In this case, the LSP is not stable, and the distinctive signature of large missing transverse momentum may therefore be lost. If only one of the λ_{ijk} is non-zero, final states with high lepton multiplicities may be produced instead. For example, a neutralino LSP will decay into two charged leptons and one neutrino:

$$\tilde{\chi}_1^0 \rightarrow \nu_{i/f} \ell_{j/i}^\pm \ell_k^\mp. \quad (2)$$

The $\tilde{\chi}_1^0$ decay proceeds via a virtual slepton or sneutrino, shown in Figure 1 for $ijk = 121$. If the lambdas are sufficiently small, sparticles are pair produced and decay via gauge interactions into LSPs. The LSPs subsequently decay via RPV interactions leading to final states with 4 leptons and non-zero MET due to the presence of neutrinos. R-parity violation releases cosmological constraints on the LSP nature [5].

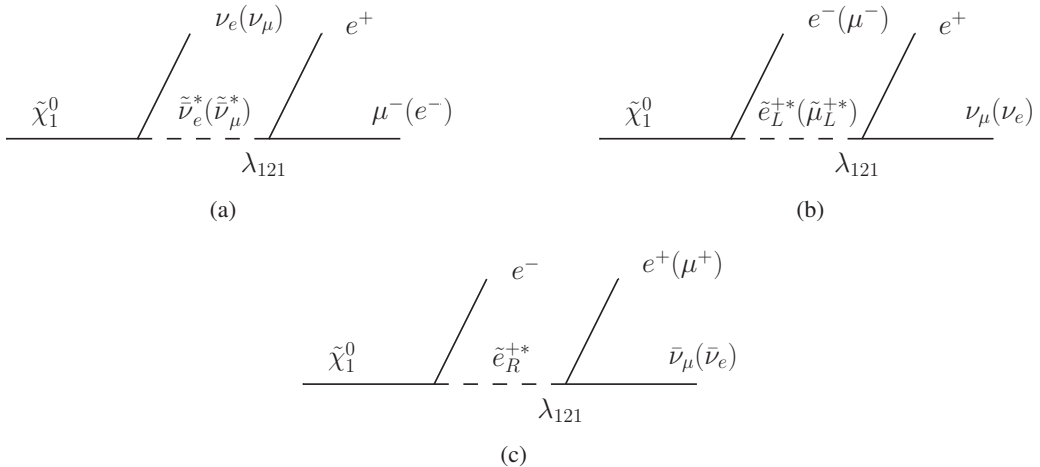


Figure 1: Illustration of $\lambda_{121} \tilde{\chi}_1^0$ decays. In all cases, the charge conjugate decay is implied.

Previous ATLAS analyses considered a model where the $\tilde{\tau}_1$ was the LSP [6, 7], however for the purposes of constructing some benchmark simplified models, a more conventional neutralino LSP is studied here. Only one RPV coupling, either λ_{121} or λ_{122} , is set to be non-zero, the exact value of that coupling being that which forces the $\tilde{\chi}_1^0$ LSP to decay promptly, with a width of 0.1 GeV irrespective of other model parameters. All other λ_{ijk} , λ'_{ijk} , λ''_{ijk} and κ_i are set to zero.

In this document, a search for new physics with a multilepton signature is presented, in events with four or more isolated leptons. The term “lepton” refers to electrons and muons only, including those from leptonic τ decays. A total of 13.0 fb^{-1} of proton-proton collision data delivered by the LHC at $\sqrt{s} = 8 \text{ TeV}$ are analysed. While motivated by supersymmetry, the search itself is model-independent. The results are presented in terms of the visible cross-section for new physics processes with this signature, and also interpreted in a variety of R-parity violating simplified supersymmetric models. This note continues and extends the analysis of Ref. [6], with improved lepton and E_T^{miss} reconstruction with respect to data taken in 2011 leading to reduced background levels and smaller systematic uncertainties. In addition, the Z-boson veto has been extended to better reject electroweak radiative decays of the Z-boson.

2 Detector description

ATLAS [8] is a multipurpose particle detector with forward-backward symmetric cylindrical geometry. It includes an inner tracker (ID) immersed in a 2 T axial magnetic field providing precision tracking of charged particles for pseudorapidities¹ $|\eta| < 2.5$. Sampling calorimeter systems with either liquid argon or scintillator tiles as the active media provide energy measurements over the range $|\eta| < 4.9$. The muon detectors are positioned outside the calorimeters and are contained in a toroidal magnetic field produced by air-cored superconducting magnets with field integrals varying from $1 \text{ T}\cdot\text{m}$ to $8 \text{ T}\cdot\text{m}$. The ID and muon detectors provide trigger and high-precision tracking capabilities for $|\eta| < 2.4$ and $|\eta| < 2.7$, respectively.

3 Event reconstruction and preselection

Events recorded during normal running conditions are analysed if the primary vertex has five or more tracks associated to it. The primary vertex of an event is identified as the vertex with the highest Σp_T^2 of associated tracks.

Electrons must satisfy “medium” identification criteria, similar to Ref. [9], and fulfil $|\eta| < 2.47$ and $E_T > 10 \text{ GeV}$, where E_T and $|\eta|$ are determined from the calibrated clustered energy deposits in the electromagnetic calorimeter and the matched ID track, respectively. Muons are reconstructed by combining tracks in the ID and tracks in the muon spectrometer [10]. Reconstructed muons are considered as candidates if they have transverse momentum $p_T > 10 \text{ GeV}$ and $|\eta| < 2.4$.

Jets are reconstructed with the anti- k_t algorithm [11] with a distance parameter of $R = 0.4$ using three-dimensional calorimeter energy clusters as input. The clusters are calibrated using local cluster calibration, consisting of weighting differently the energy deposits arising from electromagnetic showers and those from hadronic showers [12]. The final jet energy calibration includes the jet energy scale, which corrects the calorimeter response to the true particle-level jet energy [13, 14]. The correction factors were obtained from simulation and have been refined and validated using data. Jets considered in this analysis have $E_T > 20 \text{ GeV}$ and $|\eta| < 2.5$. The p_T -weighted fraction of the tracks in the jet that are associated with the primary vertex is required to be larger than 0.5.

¹ATLAS uses a right-handed coordinate system with its origin at the nominal interaction point (IP) in the centre of the detector and the z -axis along the beam pipe. The x -axis points from the IP to the centre of the LHC ring, and the y -axis points upward. Cylindrical coordinates (r, ϕ) are used in the transverse plane, ϕ being the azimuthal angle around the beam pipe. The pseudorapidity is defined in terms of the polar angle θ as $\eta = -\ln \tan(\theta/2)$.

Events containing jets failing the quality criteria described in Ref. [13] are rejected to suppress both unwanted collision and single beam background. Jets are identified as containing b -hadron decays, and thus called “ b -tagged”, using a multivariate technique based on quantities such as the impact parameters of the tracks associated to a reconstructed secondary vertex. The chosen working point of the b -tagging algorithm [15] correctly identifies b -quark jets in simulated top-quark decays with an efficiency of 85%, with a light-flavour jet misidentification rate of about 10% [16] for jets with $E_T > 20$ GeV and $|\eta| < 2.5$.

The missing transverse momentum, E_T^{miss} , is the magnitude of the vector sum of the transverse momentum or transverse energy of all $p_T > 10$ GeV muons, $E_T > 10$ GeV electrons, $E_T > 20$ GeV jets, and calibrated calorimeter energy clusters with $|\eta| < 4.9$ not associated to these objects. Reconstructed tracks are used to suppress pileup in the soft components of E_T^{miss} [17].

In this analysis, “tagged” leptons are leptons separated from each other and from candidate jets as described below. If two candidate electrons are reconstructed with $\Delta R \equiv \sqrt{(\Delta\phi)^2 + (\Delta\eta)^2} < 0.1$, the lower energy one is discarded. Candidate jets within $\Delta R = 0.2$ of an electron candidate are rejected. To suppress leptons originating from semi-leptonic decays of c - and b -quarks, all lepton candidates are required to be separated from candidate jets by $\Delta R > 0.4$. Muons undergoing bremsstrahlung can be reconstructed with an overlapping electron candidate. To reject these, tagged electrons and muons separated from jets and reconstructed within $\Delta R = 0.1$ of each other are both discarded. Events containing one or more tagged muons that have transverse impact parameter with respect to the primary vertex $|d_0| > 0.2$ mm or longitudinal impact parameter with respect to the primary vertex $|z_0| > 1$ mm are rejected to suppress cosmic muon background.

“Signal” leptons are tagged leptons for which the scalar sum of the transverse momenta of tracks within a cone of $\Delta R = 0.3$ around the lepton candidate, and excluding the lepton candidate track itself, is less than 16% (12%) of the lepton E_T for electrons (muons). Tracks selected for the electron (muon) isolation requirement defined above are those which have $p_T > 0.4$ (1.0) GeV and are associated to the primary vertex of the event. To suppress leptons originating from secondary vertices, the distance of closest approach of the lepton track to the primary vertex normalised to its uncertainty is required to be small, with $|d_0|/\sigma(d_0) < 5$ (3) for electrons (muons) and $|z_0 \sin \theta|$ must be less than 0.4 mm (1 mm) for electrons (muons). Signal electrons must also pass “tight” identification criteria, similar to Ref. [9], and the sum of the energy deposits in the calorimeter (corrected for pileup effects) within a cone of $\Delta R = 0.3$ around the electron candidate, must be less than 18% of the electron E_T .

The data sample was collected with an inclusive selection of double-lepton triggers with asymmetric and symmetric p_T thresholds. For events that are selected by the the symmetric di-muon trigger, at least two signal muons are required to have $p_T > 14$ GeV, while for the asymmetric trigger the requirements are $p_T > 18$ GeV and $p_T > 10$ GeV, requiring at least one signal muon passing each condition. In the case of the symmetric di-electron trigger, at least two signal electrons are required to have $E_T > 14$ GeV, while for the asymmetric electron trigger the requirements are $E_T > 25$ GeV and $E_T > 10$ GeV, requiring at least one signal electron passing each condition. For events that are selected using the electron-muon (muon-electron) trigger, at least one signal electron is required to have $E_T > 14$ GeV (10 GeV) and at least one signal muon to have $p_T > 10$ GeV (18 GeV). These requirements are chosen such that the overall trigger efficiency is high for the four lepton events selected in the analysis, typically close to 100%, and independent of the lepton transverse momenta within uncertainties. The same requirements are applied to the MC simulated events using the results of the trigger simulation.

4 Signal region selection

Selected events must contain four or more signal leptons. The invariant mass of any same-flavour opposite-sign (SFOS) lepton pair, m_{SFOS} , must be above 12 GeV, otherwise the lepton pair is discarded to suppress background from low-mass resonances. Z-boson candidates are vetoed by removing events

Table 1: The selection requirements for the two signal (SR) and three validation (VR) regions. The Z -candidate veto (requirement) rejects (selects) events that have a SFOS lepton pair, a SFOS+ ℓ triplet, or a combination of two SFOS pairs with mass inside the [81.2, 101.2] GeV interval.

Selection	SR1	SR2	VR1	VR2	VR3
Number of leptons	≥ 4	≥ 4	3	≥ 4	≥ 4
SFOS pair	–	–	SFOS-veto	SFOS requirement	–
Z -candidate	Z-veto	Z-veto	Z-veto	Z requirement	Z-veto
$E_T^{\text{miss}}/\text{GeV}$	> 50	–	> 50	–	< 50
$m_{\text{eff}}/\text{GeV}$	–	> 300	–	–	< 300

with pairs, triplets or quadruplets of leptons with an invariant mass inside the [81.2, 101.2] GeV interval. Lepton pairs and triplets considered for this Z -veto must contain a SFOS pair, while lepton quadruplets must consist of two SFOS pairs.

Two signal regions are then defined: a signal region with $E_T^{\text{miss}} > 50$ GeV (SR1) and one with effective mass $m_{\text{eff}} > 300$ GeV (SR2). The effective mass is defined by the scalar sum

$$m_{\text{eff}} = E_T^{\text{miss}} + \sum_{\mu} p_T^{\mu} + \sum_e E_T^e + \sum_j E_T^j, \quad (3)$$

where p_T^{μ} (E_T^e) is the transverse momentum (transverse energy) of the signal muons (electrons) and E_T^j is the transverse energy of jets with $E_T > 40$ GeV. SR1 is sensitive to scenarios where RPV LSP decays produce neutrinos in the final state, while SR2 targets models with large particle multiplicities, for example from sparticle cascade decays, and where E_T^{miss} may be small.

Three further regions are defined to validate the expected background against data. The validation regions are described in Section 7. Table 1 summarises the signal and validation region definitions.

5 Standard Model background estimation

Several SM processes, which are classified into irreducible and reducible components below, contribute to the background in the signal regions. The dominant sources are ZZ , tribosons, WZ , and $t\bar{t}$ production in both SR1 and SR2.

5.1 Monte Carlo simulation for SM processes

Several Monte Carlo (MC) generators are used to simulate SM processes relevant for this analysis. SHERPA [18] is used to simulate the diboson processes WW , WZ and ZZ , where Z also includes virtual photons. These diboson samples correspond to all SM diagrams leading to the $\ell\nu\ell'\nu'$, $\ell\ell\ell'\nu'$, and $\ell\ell\ell'\ell'$ final states, where $\ell, \ell' = e, \mu, \tau$ and $\nu, \nu' = \nu_e, \nu_{\mu}, \nu_{\tau}$. Interference between the diagrams is taken into account. MadGraph [19] is used for the $t\bar{t}W$, $t\bar{t}WW$, $t\bar{t}Z$, $W\gamma$ and $Z\gamma$ processes. The “triboson” processes, WWW and ZWW are also simulated using MadGraph. POWHEG [20] is chosen for the simulation of the pair production of top quarks, MC@NLO and AcerMC [21] are used for the simulation of single top production, and ALPGEN [22] is used to simulate W +jets and Z +jets processes. Expected diboson yields are normalised using next-to-leading-order (NLO) QCD predictions obtained with MCFM [23, 24]. Triboson contributions are normalised to NLO predictions [25]. The top-quark pair-production contribution is normalised to approximate next-to-next-to-leading-order calculations (NNLO) [26] and the $t\bar{t}W$, $t\bar{t}WW$,

$t\bar{t}Z$ contributions are normalised to NLO predictions [27, 28]. NNLO FEWZ [29, 30] cross-sections are used for normalisation of the inclusive W +jets and Z +jets processes.

The choice of the parton distribution functions (PDFs) depends on the generator. The CTEQ6L1 [31] PDFs are used with **MadGraph** and **ALPGEN**, and the CT10 [32] PDFs with **MC@NLO** and **SHERPA**.

Fragmentation and hadronisation for the **ALPGEN** and **MC@NLO** samples are performed with **HERWIG**, while **PYTHIA** [33] is used for **MadGraph** and **POWHEG**, and for **SHERPA** these are performed internally. **JIMMY** [34] is interfaced to **HERWIG** for simulation of the underlying event. For all MC samples, the propagation of particles through the ATLAS detector is modelled using **GEANT4** [35] using the full ATLAS detector simulation [36] (except the $t\bar{t}$ **POWHEG** sample which uses fast detector simulation **AtlFast-II** [37]). The effect of multiple proton-proton collisions from the same or different bunch crossings is incorporated into the simulation by overlaying additional minimum-bias events generated with **PYTHIA** onto hard-scatter events. Simulated events are weighted to match the distribution of the number of interactions per bunch crossing observed in data, but are otherwise reconstructed in the same manner as data.

5.2 Irreducible background processes

A background process is considered “irreducible” if it leads to events with four leptons from Z/W boson, t -quark or τ decays, referred to as “real” leptons below. These include ZZ , $t\bar{t}Z$, $t\bar{t}WW$, and ZWW production, where a gauge boson may be produced off-mass-shell. These contributions are determined using the corresponding MC samples, for which lepton and jet selection efficiencies [13, 38–40] are corrected to account for differences with respect to data. The validation of the simulation of the most important background processes in Section 7 is performed, using dedicated event selection criteria designed to enhance these processes.

5.3 Reducible background processes

A “reducible” process has at least one “fake” lepton, that is either a lepton from a semi-leptonic decay of a b - or c -quark, referred to as heavy-flavour, a lepton from misidentified light-flavour quark or gluon jet, referred to as light-flavour, or an electron from an isolated single-track photon conversion. The reducible background includes WZ , $t\bar{t}$, $t\bar{t}W$, WW , single t -quark, or single Z -boson production, in many cases produced in association with jets or photons. MC simulation studies show that the WZ and the $t\bar{t}W$ backgrounds correspond respectively to 95% and 5% of the reducible background in SR1 and SR2 and that the yield of W bosons with three fake leptons is negligible. In both SR1 and SR2, fake leptons are predominantly fake electrons (90%), originating from photon conversions, with a small contribution of fake electrons from light-flavour. Fake muons from heavy flavour (b and c quark) decays and light-flavour are suppressed by the object separation scheme described in Section 3, while fake muons from photon conversions are rare. As the overall contribution from heavy-flavour jets is small, the combination of light- and heavy-flavour fakes are grouped together as “jet fakes” in what follows.

The reducible background is estimated using a weighting method applied to events containing signal leptons (ℓ_S) and loose leptons (ℓ_L), which are tagged leptons failing the signal lepton requirements. Since the reducible background is dominated by events with at most two fake leptons, it is estimated as:

$$\begin{aligned} & [N_{\text{data}}(3\ell_S + \ell_L) - N_{\text{MCirr}}(3\ell_S + \ell_L)] \times F(\ell_L) \\ & - [N_{\text{data}}(2\ell_S + \ell_{L_1} + \ell_{L_2}) - N_{\text{MCirr}}(2\ell_S + \ell_{L_1} + \ell_{L_2})] \times F(\ell_{L_1}) \times F(\ell_{L_2}), \end{aligned} \quad (4)$$

where the second term corrects for the double counting of reducible-background events with two fake leptons in the first term. The term $N_{\text{data}}(3\ell_S + \ell_L)$ is the total number of events with three signal leptons and one loose lepton, while $N_{\text{MCirr}}(3\ell_S + \ell_L)$ is the irreducible contribution of events obtained from

simulation. The definitions of $N_{\text{data}}(2\ell_S + \ell_{L_1} + \ell_{L_2})$ and $N_{\text{MCirr}}(2\ell_S + \ell_{L_1} + \ell_{L_2})$ are analogous, except that the two loose leptons are explicitly numbered (ℓ_{L_1} and ℓ_{L_2}). The potential signal contamination in the $3\ell_S + \ell_L$ and $2\ell_S + \ell_{L_1} + \ell_{L_2}$ loose lepton data samples is not taken into account, which leads to a conservative discovery potential and has negligible effect on the exclusion limits as the reducible background contribution in the signal regions is smaller than the uncertainties as shown in Section 8. The average fake ratio of signal to loose leptons, F , depends on the flavour and kinematics of the loose lepton ℓ_L and it is defined as:

$$F = \sum_{i,j} (\alpha^i \times R^{ij} \times f^{ij}), \quad (5)$$

where i is the type of fake (jet fakes or electrons from photon conversion) and j is the process category the fake originates from (top quark or W/Z boson). The fake ratios f^{ij} are defined as the ratios of the probabilities that fake tagged leptons are identified as signal leptons to the probabilities that they are identified as loose leptons. The f^{ij} are determined for each relevant fake type and for each reducible-background process, and they are parameterised in muon (electron) p_T (E_T) and η . The fake ratios are weighted according to the fractional contribution of the process they originate from through R^{ij} fractions. Both f^{ij} and R^{ij} are determined from simulation. Each correction factor α^i is the fake ratio measured in data divided by that in simulation, in control samples described below. They are all found to have no significant dependence on the lepton p_T . The fake ratios F are estimated to vary from 0.2 to 0.6 for muons from jets in boson processes, when the muon p_T increases from 10 to 100 GeV. For muons from jets in top-quark processes, the same fake ratio decreases from 0.10 to 0.06 over the same p_T range. For electrons, the fake ratios F increase from 0.02 to 0.10 (0.05 to 0.3) for electrons from jets in top-quark/boson processes (from photon conversions) when the electron p_T increases from 10 to 100 GeV. The electron fake ratio can be lower than the muon fake ratio due to the additional identification criteria applied to electrons.

The correction factor for heavy-flavour jet fakes is measured in a $b\bar{b}$ -dominated control sample defined by selecting events with only one b -tagged jet (containing a muon) and a tagged lepton. The non- $b\bar{b}$ contributions from the single and pair production of top quarks and W bosons produced in association with b -quarks are suppressed with $E_T^{\text{miss}} < 60$ GeV and transverse mass $m_T < 50$ GeV requirements, where $m_T = \sqrt{2 \cdot E_T^{\text{miss}} \cdot p_T^\ell \cdot (1 - \cos \Delta\phi_{\ell, E_T^{\text{miss}}})}$ and $\Delta\phi_{\ell, E_T^{\text{miss}}}$ is the azimuthal angle between the tagged lepton ℓ and E_T^{miss} . The remaining non- $b\bar{b}$ background ($\sim 1\%$ level) is subtracted from the control sample in data using MC predictions. In this control sample, the fake ratio for leptons from heavy-flavour jets is calculated using the ratio of tagged leptons passing signal lepton requirements to those that fail. The correction factors are found to be 0.70 ± 0.04 and 0.81 ± 0.04 for electrons and muons respectively.

The contribution of fake leptons from light-flavour jets is expected to be negligible in this analysis. Nevertheless, the light-flavour correction factor is measured in a Z + light-flavour jets dominated control sample to cross-check the MC simulation. Events with two SFOS leptons and one tagged lepton of different flavour (i.e. $e^+e^- + \mu$ or $\mu^+\mu^- + e$) are selected and the invariant mass of the SFOS pair is required to lie within 10 GeV of the nominal Z -boson mass value. The three leptons in the event must be separated from all other leptons and jets in the event by $\Delta R > 0.4$ and events with b -tagged jets are rejected. To suppress leptons originating from photon conversions, the trilepton mass is required to lie outside 10 GeV of the nominal Z -boson mass value. Finally, $E_T^{\text{miss}} < 20$ GeV is required to suppress non- Z backgrounds. In this control sample, the fake ratio for leptons from light-flavour jets is calculated using the ratio of tagged leptons identified as signal leptons to those identified as loose leptons. The correction factor is found to be 1.50 ± 0.29 for electrons and 1.07 ± 0.27 for muons.

The correction factor for electron candidates originating from photon conversions is determined in a sample of photons radiated from a muon in $Z \rightarrow \mu\mu$ decays. Events with two opposite-sign muons and one tagged electron are selected and the invariant mass of the $\mu\mu e$ triplet is required to lie within 10 GeV of the nominal Z -boson mass value. In this control sample, the fake ratio for electrons from

photon conversions is calculated using the ratio of tagged electrons identified as signal electrons to those identified as loose electrons. The correction factor is found to be 1.06 ± 0.30 .

6 Systematic uncertainties

Several sources of systematic uncertainty are considered in the signal, control and validation regions. Correlations of systematic uncertainties between processes and regions are accounted for.

Uncertainties on the MC simulation affect the irreducible background estimate, the R^{ij} fractions of the average fake ratios, and the signal yields. Theoretical uncertainties on the cross-sections include PDF uncertainties, estimated using appropriate PDF error sets, and uncertainties on the renormalisation and factorisation scales, estimated by varying each by a factor of one half and two. Uncertainties on the acceptance from PDFs are also taken into account, and are small relative to the leading systematic uncertainties. Additional systematic uncertainties are those resulting from the jet energy scale [13] and resolution [38], the lepton efficiencies [39, 40], energy scales and resolutions, and uncertainties in b -tagging rates [16, 41]. The impact of the choice of MC generator is estimated for the irreducible background. The systematic uncertainty on the luminosity is 3.6%, measured using a technique similar to that of [42, 43] and affects only the yields of the irreducible background and the signal. A 5% uncertainty is applied to MC samples to cover differences in efficiency seen between the trigger in data and the MC trigger simulation.

In SR1 (SR2), the total uncertainty on the irreducible background is about 100% (45%). This is dominated by the uncertainties on the MC modeling of the ZZ background, estimated by computing the difference in acceptance obtained with SHERPA (nominal) and POWHEG generators. Additional significant uncertainties on the ZZ contribution arise from the jet energy scale and the statistics of the MC. For the other irreducible backgrounds, the theoretical uncertainties on the cross-section are the most important. A 50% cross-section uncertainty is assumed for $t\bar{t}Z$ [27] and $t\bar{t}WW$, and a conservative 100% uncertainty is assumed for triboson processes.

For the average fake ratio F , the R^{ij} fractions are varied between 0% and 100%, providing a conservative uncertainty on the R^{ij} fractions from the sources listed above. This constitutes the dominant systematic uncertainty on the reducible background, of order 50% to 100%, depending on the lepton kinematics. In validation regions requiring only three leptons, the uncertainties on the fractions are known to a better degree but this conservative approach is used for consistency across regions. Uncertainties related to possible dependence of the fake ratios on E_T^{miss} , as determined in simulation, and uncertainties on the scale factors are also taken into account. Due to the small event counts in the control regions, statistical uncertainties are also important.

7 Background model validation

The background expectations have been verified in three validation regions. A region (VR1) selects events with three signal leptons, no SFOS pair among the three leptons and $E_T^{\text{miss}} > 50 \text{ GeV}$. Events in VR1 are dominated by $t\bar{t}$ production, and this region is used to validate the reducible background estimate. The contribution from ZZ production is validated in a region (VR2) defined by events with four leptons containing a Z -boson candidate, as described in Section 4. A region (VR3) containing events with $E_T^{\text{miss}} < 50 \text{ GeV}$, $m_{\text{eff}} < 300 \text{ GeV}$, four signal leptons, and no Z -boson candidate is used to validate the simulation of off-shell Z -bosons. The data and background expectations are found to be in agreement within the quoted statistical and systematic uncertainties, as shown in Table 2. The CL_b value [44], testing compatibility with the background prediction, is also reported in each region. The distribution of E_T^{miss} , m_{eff} , and the p_T of the leptons in VR1 and VR2 are shown in Figures 2–5, where good agreement is seen between data and background expectation.

Table 2: Expected number of events from SM backgrounds and observed number of events in data in validation regions VR1, VR2 and VR3 (13.0 fb^{-1}). The uncertainties quoted include statistical and systematic sources. The processes labelled with (\dagger) are classified as irreducible background in the three-lepton validation regions. In the four-lepton validation regions they are included in the reducible background. The CL_b value is also given for each region [44].

Selection	VR1	VR2	VR3
ZZ	$0.43^{+0.32}_{-0.32}$	135^{+13}_{-13}	$3.9^{+1.7}_{-1.7}$
ZWW	$0.29^{+0.29}_{-0.29}$	$1.2^{+1.2}_{-1.2}$	$0.018^{+0.018}_{-0.018}$
$t\bar{t}Z$	$0.44^{+0.23}_{-0.23}$	$2.0^{+1.0}_{-1.0}$	$0.011^{+0.011}_{-0.011}$
$t\bar{t}WW$	$0.057^{+0.031}_{-0.031}$	$(2.5^{+2.3}_{-2.3}) \times 10^{-3}$	$(4^{+1}_{-4}) \times 10^{-3}$
$WZ (\dagger)$	$4.4^{+0.9}_{-0.8}$	–	–
$t\bar{t}W (\dagger)$	$2.1^{+0.7}_{-0.7}$	–	–
$WWW (\dagger)$	$1.9^{+1.9}_{-1.9}$	–	–
Irreducible Bkg.	10^{+4}_{-4}	138^{+15}_{-15}	$3.9^{+1.7}_{-1.7}$
Reducible Bkg.	19^{+46}_{-6}	$1.2^{+1.5}_{-1.2}$	$0.0^{+0.40}_{-0.0}$
Total Bkg.	29^{+46}_{-7}	139^{+14}_{-14}	$3.9^{+1.5}_{-1.5}$
Data	35	159	0
CL_b	0.56	0.86	0.08

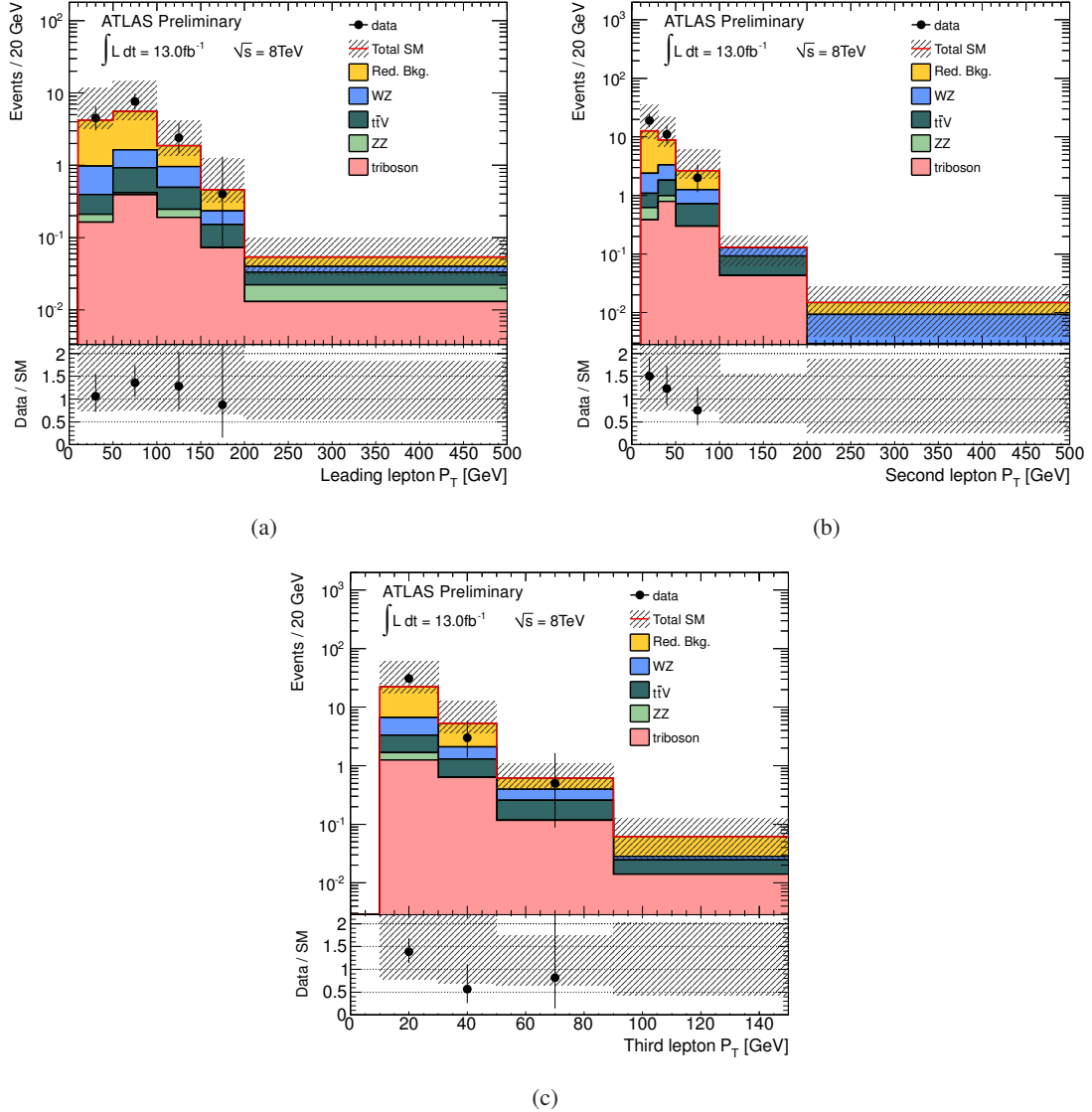


Figure 2: Distributions of the p_T of (a) the leading lepton, (b) the second leading lepton and (c) the third leading lepton for events in VR1. The ratio of data to the SM prediction is also shown. The uncertainty band includes both statistical and systematic uncertainty.

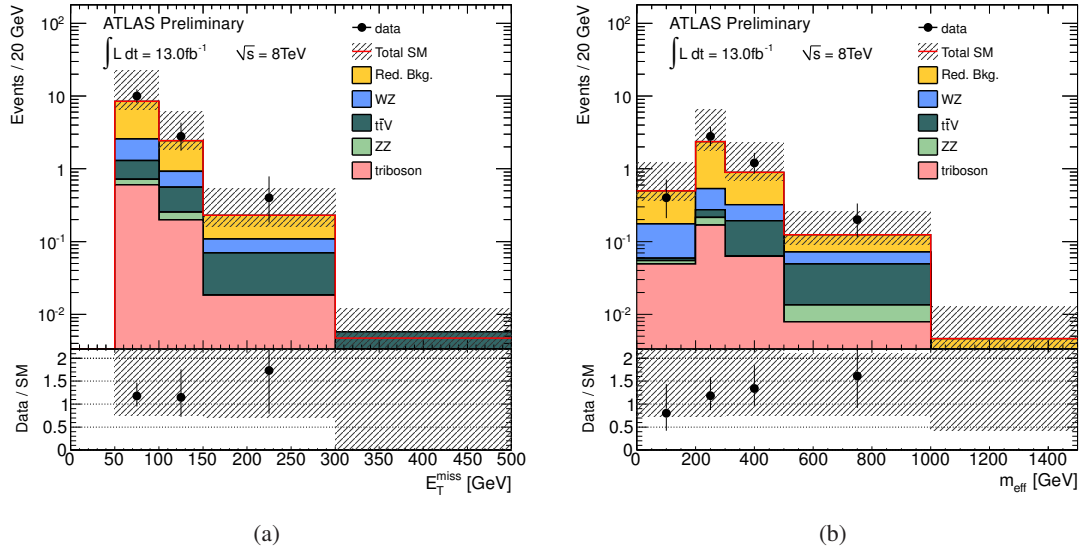


Figure 3: Distributions of (a) E_T^{miss} and (b) m_{eff} for events in VR1. The ratio of data to the SM prediction is also shown. The uncertainty band includes both statistical and systematic uncertainty.

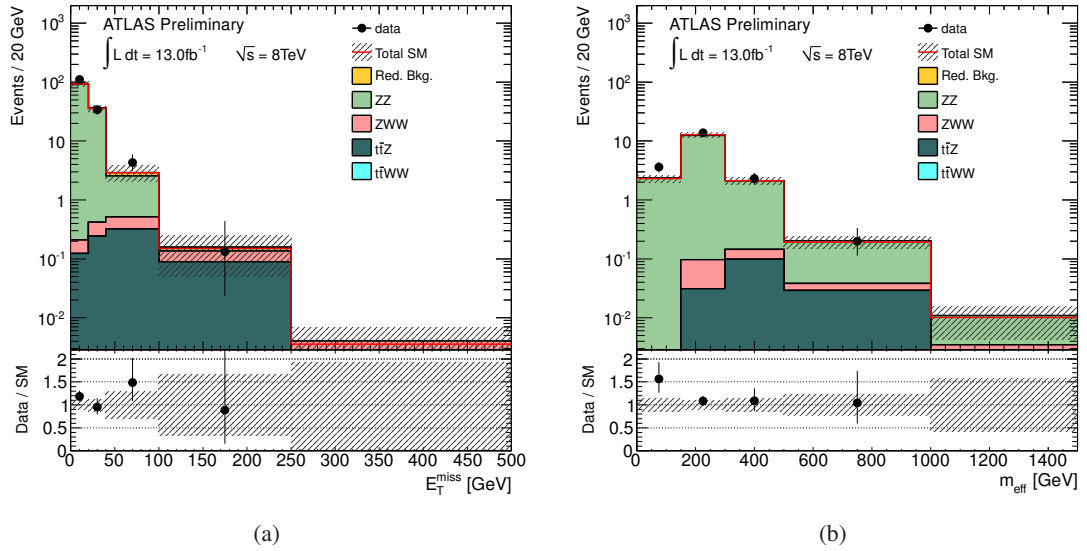


Figure 4: Distributions of (a) E_T^{miss} and (b) m_{eff} for events in VR2. The ratio of data to the SM prediction is also shown. The uncertainty band includes both statistical and systematic uncertainty.

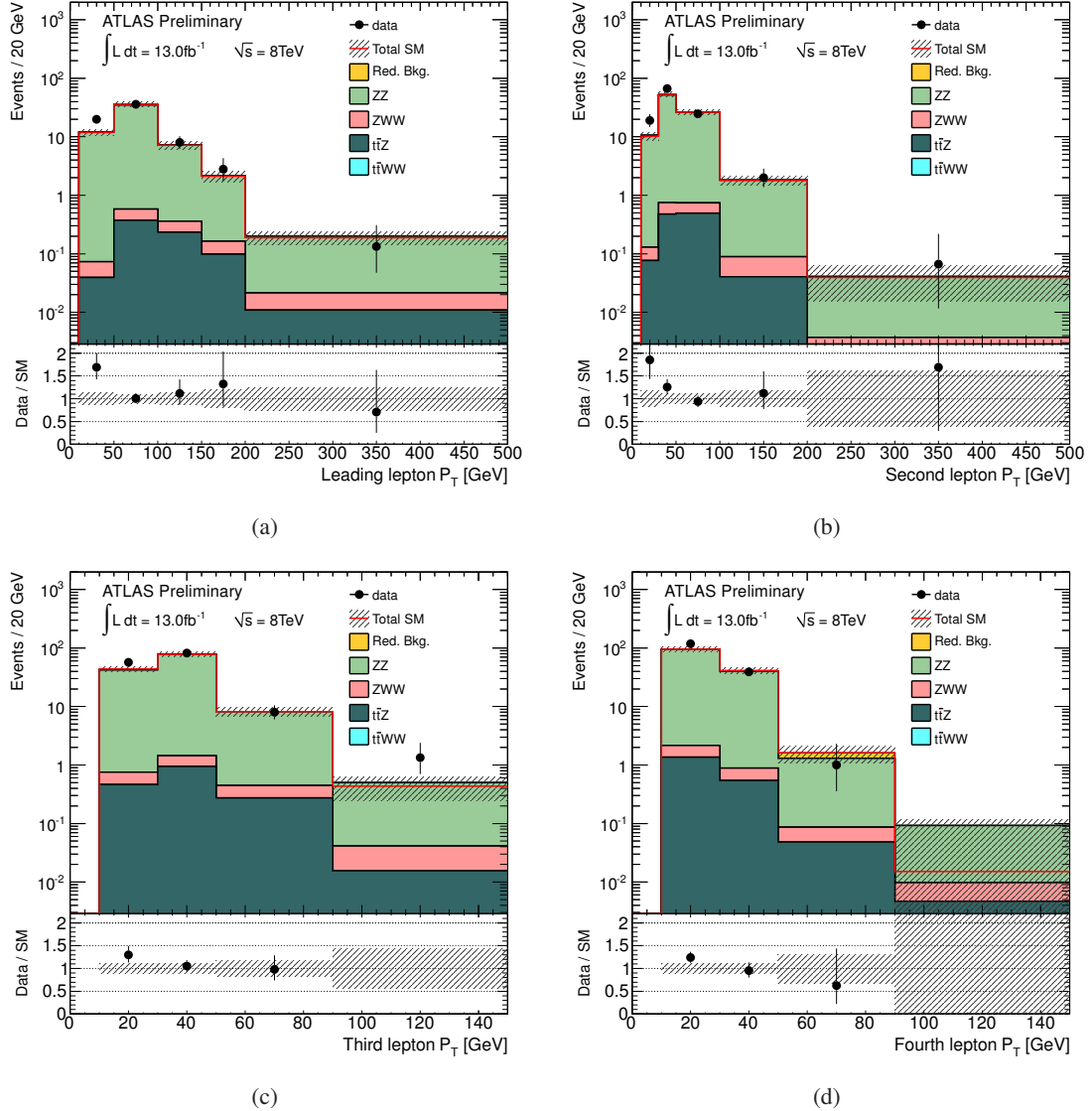


Figure 5: Distributions of the p_T of (a) the leading lepton, (b) the second leading lepton, (c) the third leading lepton and (d) the fourth leading lepton for events in VR2. The ratio of data to the SM prediction is also shown. The uncertainty band includes both statistical and systematic uncertainty.

8 Results

The numbers of observed and expected events in SR1 and SR2 are reported in Table 3. No significant excess of events is found in the signal regions.

Upper limits on the visible cross-section of new physics processes are calculated, defined by the product of production cross-section, acceptance and efficiency, and placed at 95% CL with the modified frequentist CL_s prescription [44]. All systematic uncertainties and their correlations are taken into account via nuisance parameters in a profile likelihood fit [45]. Observed 95% CL limits on the visible cross-section are placed at 0.34 fb in SR1 and 0.38 fb in SR2. The corresponding expected limit is 0.28 fb in both regions. The calculated probability that the signal-free background fluctuates to the observed number of events or higher is 3.7% in SR1 and 16% in SR2.

Table 3: Expected number of events from SM backgrounds, and observed number of events in data in signal regions SR1 and SR2 (13.0 fb^{-1}). The uncertainties quoted include statistical and systematic effects. The quoted p_0 -values show the probability of the background fluctuating to the observed number of events or higher, also given in standard deviations (σ). Upper limits on the observed and expected visible production cross-section of new physics processes at 95% CL, σ_{vis} , are also shown.

Selection	SR1	SR2
ZZ	$0.07^{+0.22}_{-0.07}$	$1.0^{+0.4}_{-0.4}$
ZWW	$0.10^{+0.10}_{-0.10}$	$0.09^{+0.09}_{-0.09}$
$t\bar{t}Z$	$0.045^{+0.028}_{-0.028}$	$0.06^{+0.04}_{-0.04}$
$t\bar{t}WW$	$(6^{+6}_{-5}) \times 10^{-3}$	$(3.3^{+4.8}_{-3.3}) \times 10^{-3}$
Irreducible Bkg.	$0.22^{+0.27}_{-0.21}$	$1.1^{+0.5}_{-0.4}$
Reducible Bkg.	$0.028^{+0.107}_{-0.028}$	$0.10^{+0.14}_{-0.10}$
Total Bkg.	$0.25^{+0.29}_{-0.25}$	$1.2^{+0.5}_{-0.4}$
Data	1	2
p_0 -value (σ)	0.037 (1.8)	0.16 (1.0)
σ_{vis} (exp)	$< 0.28 \text{ fb}$	$< 0.28 \text{ fb}$
σ_{vis} (obs)	$< 0.34 \text{ fb}$	$< 0.38 \text{ fb}$

9 Interpretation in RPV simplified models

The above results are interpreted in the context of eight RPV simplified models, all with the signature of a neutralino LSP decaying as described in Section 1. As this analysis is only sensitive to first- and second-generation leptons, the focus is restricted to λ_{121} and λ_{122} LSP decays. Direct LSP pair production is in principle detectable, however the production cross-section is found to be vanishingly small unless specific Wino/Higgsino mixing is assumed. Therefore, models are analysed that include one or more next-to-lightest SUSY particle (NLSP), produced in pairs, where each NLSP decays promptly to the LSP in a prescribed manner. All sparticles other than the LSP and NLSP(s) have masses set to 4.5 TeV. Possible small changes in acceptance of the LSP decays due these sparticles are neglected.

Four NLSP choices are considered in this analysis, with the following constituents and cascade decays:

Winos: only $\tilde{\chi}_1^\pm$ is considered, where $\tilde{\chi}_1^\pm \rightarrow W^\pm \tilde{\chi}_1^0$ (the gauge boson may be virtual).

L-sleptons: equal-mass \tilde{e}_L , $\tilde{\mu}_L$ and $\tilde{\tau}_L$, where $\tilde{\ell}_L \rightarrow \ell \tilde{\chi}_1^0$.

Sneutrinos: equal-mass $\tilde{\nu}_e$, $\tilde{\nu}_\mu$ and $\tilde{\nu}_\tau$, where $\tilde{\nu}_\ell \rightarrow \nu_\ell \tilde{\chi}_1^0$.

Gluino: $\tilde{g} \rightarrow q \bar{q}' \tilde{\chi}_1^0$ ($q, \bar{q}' \in u, d, s, c$).

Three of the models focus on electroweak sparticle production, as this will lead to the most conservative limits, while the gluino model serves as an example of how the experimental reach increases for strong production processes.

Relevant experimental limits from previous SUSY searches exist for all the models considered in this note. The Wino model used in this analysis is similar to one considered by D0 [46], where limits were placed on Wino-like $\tilde{\chi}_1^\pm$ and $\tilde{\chi}_2^0$ of approximately 220 GeV for non-zero λ_{121} and λ_{122} couplings. For the case of a non-zero λ_{121} , these limits were extended up to approximately 540 GeV by ATLAS using data taken in 2011 [6]. The principal difference between that model and the one used here is that $\tilde{\chi}_2^0$ production processes are not considered in this note. The LEP experiments placed limits on slepton and sneutrino masses in leptonic RPV scenarios [47]. The results vary slightly depending on the slepton or sneutrino flavour, but all are of order 100 GeV [48]. CMS has placed limits in a squark and gluino co-NLSP model with leptonic R-parity violation. With a non-zero λ_{123} coupling, they exclude gluino masses below 1 TeV, assuming $m_{\tilde{\chi}_1^0} = 300$ GeV [49]. This coupling will produce a significant number of tau leptons in the final state, but is otherwise similar to the model considered here.

The simplified model samples studied here are produced with *Herwig++* [50]. Signal cross-sections are calculated to NLO in the strong coupling constant using *PROSPINO*². The nominal cross-section and the uncertainty are taken from an envelope of cross-section predictions using different PDF sets and factorisation and renormalisation scales, as described in Ref. [56]. For Wino, slepton and sneutrino production, the theoretical uncertainties are modest, varying from approximately 5% at low NLSP masses to about 10% for the highest masses considered. The uncertainties on gluino production are much greater, due to increased PDF uncertainties, ranging from 16% at $m_{\tilde{g}} = 500$ GeV to nearly 60% at $m_{\tilde{g}} = 1700$ GeV.

The requirements on the minimum value of the SFOS dilepton mass and on the minimum lepton-lepton separation reduce the acceptance and selection efficiency for leptons from the light $\tilde{\chi}_1^0$. In addition, as the mass of the $\tilde{\chi}_1^0$ approaches zero, the phase space for leptonic decays is greatly reduced, decreasing the likelihood of a prompt LSP decay. For these reasons, only LSP masses greater than 10 GeV are considered (50 GeV for sneutrino and gluino models). For similar reasons when considering the NLSP decay, the focus is restricted to $m_{\tilde{\chi}_1^0} < m_{\text{NLSP}} - 10$ GeV. The NLSP mass range considered varies, depending on current constraints and our expected sensitivity to each model.

The distributions of the E_T^{miss} in SR1 and the m_{eff} in SR2 are presented in Figure 6, where the expectation from one sample mass point from the Wino model is included for illustration purposes. The separation of signal and background events that both of these variables achieve can clearly be seen.

Exclusion limits on the models described above are reported in Figures 7 to 10, where the 95 % CL limits are calculated choosing the signal region with the best expected limit for each of the model points. Across most of every plane, SR1 is more sensitive than SR2. The uncertainties on the signal cross-section are not included in the limit calculation but their impact on the observed limit is shown. Quoted exclusion limits on sparticle masses refer to the lower edge of the theoretical uncertainty band. In the Wino models

²The addition of the resummation of soft gluon emission at NLL [51–55] is performed in the case of the gluino model.

(Figure 7), NLSP masses of up to ~ 710 GeV are excluded, depending on the $\tilde{\chi}_1^0$ mass, for both λ_{121} and λ_{122} LSP decays. For $m_{\tilde{\chi}_1^0} > 150$ GeV, this limit has only a weak dependence on the LSP mass. As the $\tilde{\chi}_1^0$ mass decreases, the limit rapidly weakens to approximately 300 GeV for $m_{\tilde{\chi}_1^0} = 10$ GeV. This general pattern is repeated across all of the models, with maximum excluded masses of approximately 450 GeV for left-handed sleptons, and 1300 GeV for gluinos.

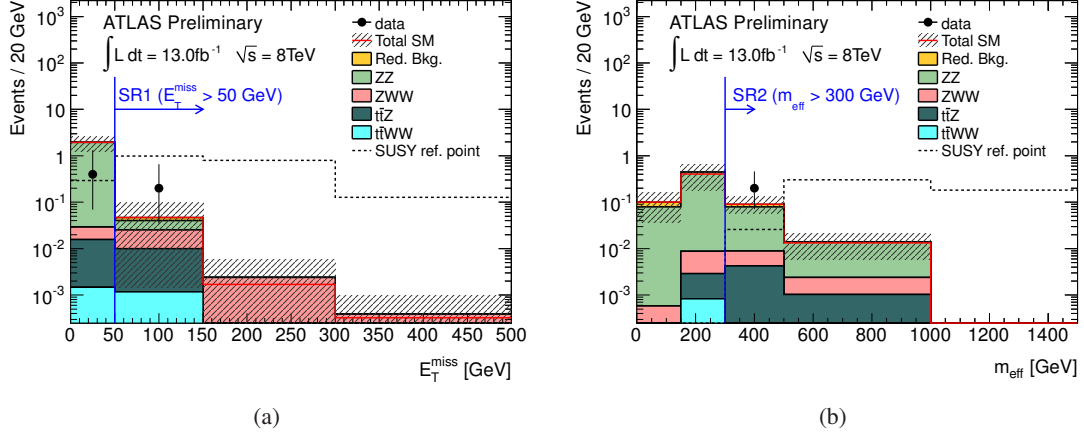


Figure 6: Distributions of (a) E_T^{miss} and (b) m_{eff} in events with at least four leptons and no Z boson candidates. Events in (a) with $E_T^{\text{miss}} > 50$ GeV are those in SR1, while events in (b) with $m_{\text{eff}} > 300$ GeV are those in SR2. The uncertainty band includes both statistical and systematic uncertainty. The yield of one benchmark SUSY model is shown for illustration purposes. “SUSY ref. point” is a scenario from the RPV Wino λ_{121} simplified model, with $m_{\tilde{\chi}_1^{\pm}} = 600$ GeV, $m_{\tilde{\chi}_1^0} = 400$ GeV. The signal distribution is not stacked on top of the expected background.

10 Summary

Results from a search for new phenomena in the final state with four or more leptons (electrons or muons), no Z candidates, and either moderate values of missing transverse momentum or large effective mass are reported. The analysis is based on 13.0 fb^{-1} of proton-proton collision data delivered by the LHC at $\sqrt{s} = 8$ TeV. No significant excess of events is found in data. Observed 95% CL limits on the visible cross-section are placed at 0.34 fb and 0.38 fb in the two signal regions used in this analysis. The null result is interpreted in a range of simplified models in which the lightest neutralino decays promptly into two charged leptons and a neutrino via an RPV coupling. In the Wino simplified model of RPV supersymmetry, chargino masses up to 710 GeV are excluded. Limits on other NLSP choices are: up to ~ 450 GeV for left-handed sleptons, up to ~ 410 GeV for sneutrinos, and up to ~ 1300 GeV for gluinos.

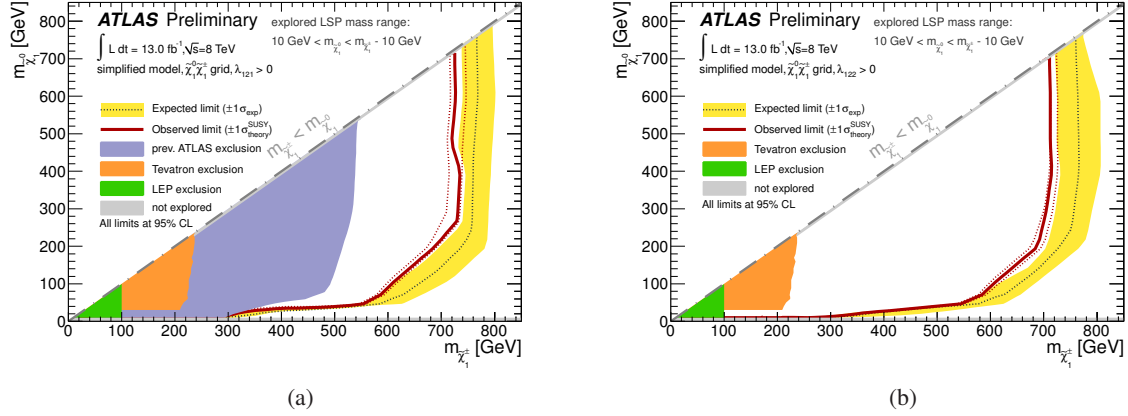


Figure 7: Observed and expected 95% CL limit contours for the RPV Wino simplified model where (a) $\lambda_{121} > 0$ and (b) $\lambda_{122} > 0$. The expected and observed limits are calculated without signal cross-section uncertainty taken into account. The yellow band is the $\pm 1\sigma$ experimental uncertainty on the expected limit. The red dashed band is the $\pm 1\sigma$ signal theory uncertainty on the observed limit. The exclusion contours are optimized by applying in each signal grid point the CL values from the most sensitive signal region (lowest expected CL). Previous exclusion limits are shown from ATLAS [6], D0 [46] and the LEP experiments [47].

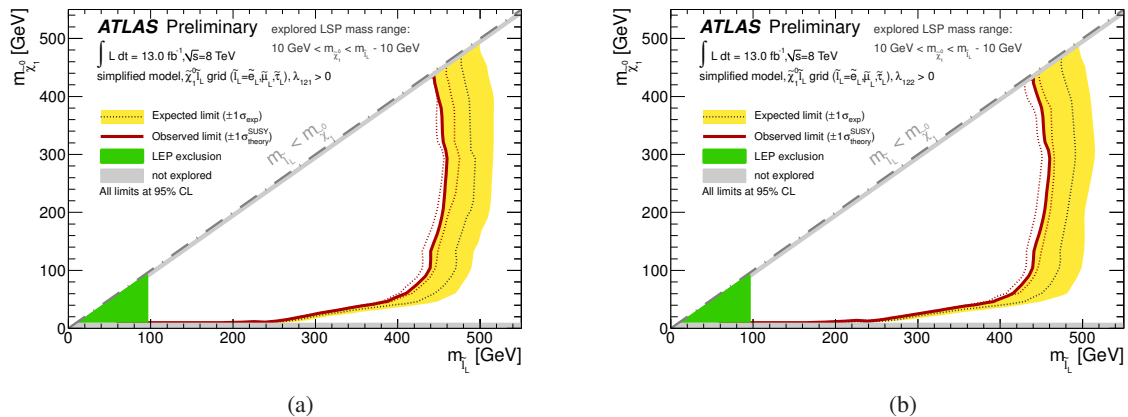


Figure 8: Observed and expected 95% CL limit contours for the RPV L-slepton simplified model where (a) $\lambda_{121} > 0$ and (b) $\lambda_{122} > 0$. For further details, refer to Figure 7. Limits from LEP on slepton masses in RPV scenarios are reported in Refs. [47, 48].

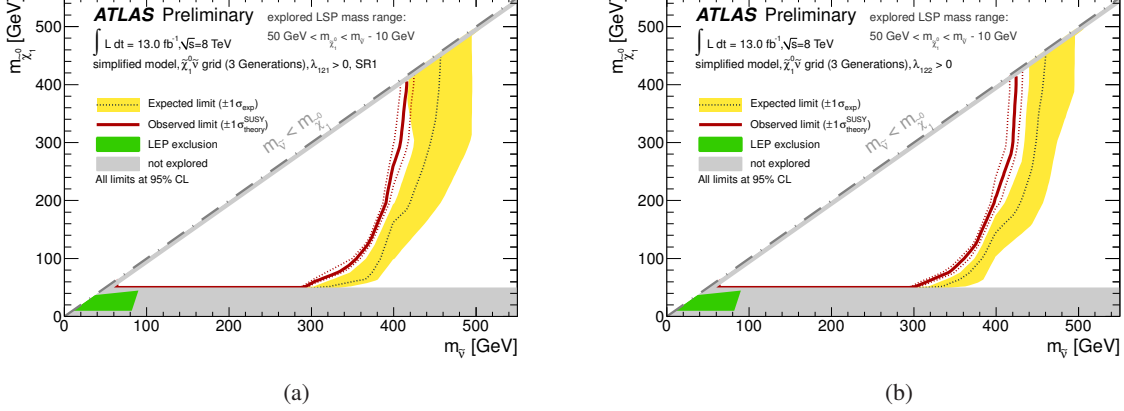


Figure 9: Observed and expected 95% CL limit contours for the RPV sneutrino simplified model where (a) $\lambda_{121} > 0$ and (b) $\lambda_{122} > 0$. For further details, refer to Figure 7. Limits from LEP on sneutrino masses in RPV scenarios are reported in Refs. [47, 48].

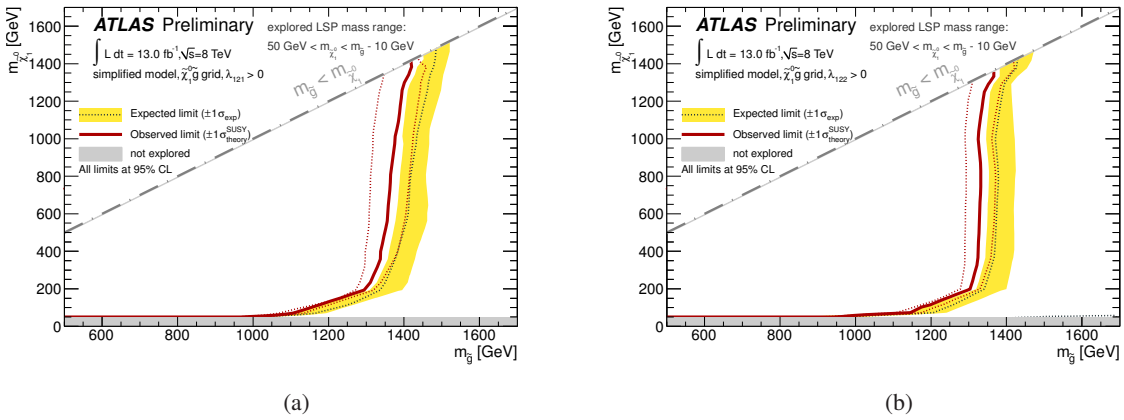


Figure 10: Observed and expected 95% CL limit contours for the RPV gluino simplified model where (a) $\lambda_{121} > 0$ and (b) $\lambda_{122} > 0$. For further details, refer to Figure 7.

References

- [1] H. Miyazawa, *Prog. Theor. Phys.* **36** (6) (1966) 1266–1276.
P. Ramond, *Phys. Rev.* **D3** (1971) 2415–2418.
- Y. A. Gol’fand and E. P. Likhtman, *JETP Lett.* **13** (1971) 323–326. [*Pisma Zh.Eksp.Teor.Fiz.* 13:452-455,1971].
- A. Neveu and J. H. Schwarz, *Nucl. Phys.* **B31** (1971) 86–112.
- A. Neveu and J. H. Schwarz, *Phys. Rev.* **D4** (1971) 1109–1111.
- J. Gervais and B. Sakita, *Nucl. Phys.* **B34** (1971) 632–639.
- D. V. Volkov and V. P. Akulov, *Phys. Lett.* **B46** (1973) 109–110.
- J. Wess and B. Zumino, *Phys. Lett.* **B49** (1974) 52–54.
- J. Wess and B. Zumino, *Nucl. Phys.* **B70** (1974) 39–50.
- [2] S. Weinberg, *Phys. Rev.* **D26** (1982) 287–302.
N. Sakai and T. Yanagida, *Nucl. Phys.* **B197** (1982) 533–542.
- [3] P. Fayet, *Phys. Lett.* **B64** (1976) 159–162.
P. Fayet, *Phys. Lett.* **B69** (1977) 489–494.
G. R. Farrar and P. Fayet, *Phys. Lett.* **B76** (1978) 575–579.
P. Fayet, *Phys. Lett.* **B84** (1979) 416–420.
S. Dimopoulos and H. Georgi, *Nucl. Phys.* **B193** (1981) 150–162.
- [4] H. Goldberg, *Phys. Rev. Lett.* **50** (1983) 1419–1422.
J. Ellis et al., *Nucl. Phys.* **B238** (1984) 453–476.
- [5] H. K. Dreiner and S. Grab, *Phys. Lett.* **B679** (2009) 45–50, [arXiv:0811.0200](https://arxiv.org/abs/0811.0200) [hep-ph].
- [6] ATLAS Collaboration, submitted to *JHEP* (2012), [arXiv:1210.4457](https://arxiv.org/abs/1210.4457) [hep-ex].
- [7] ATLAS Collaboration, ATLAS-CONF-2012-035.
<https://cdsweb.cern.ch/record/1432202>.
- [8] ATLAS Collaboration, *JINST* **3** (2008) S08003.
- [9] ATLAS Collaboration, *Eur. Phys. J.* **C72** (2012) 1909, [arXiv:1110.3174](https://arxiv.org/abs/1110.3174) [hep-ex].
- [10] ATLAS Collaboration, ATLAS-CONF-2012-143.
<https://cdsweb.cern.ch/record/1491697>.
- [11] M. Cacciari et al., *JHEP* **0804** (2008) 063, [arXiv:0802.1189](https://arxiv.org/abs/0802.1189) [hep-ph].
- [12] ATLAS Collaboration, p.266-273, [arXiv:0901.0512](https://arxiv.org/abs/0901.0512) [hep-ex].
- [13] ATLAS Collaboration, [arXiv:1112.6426](https://arxiv.org/abs/1112.6426) [hep-ex].
- [14] ATLAS Collaboration, [arXiv:1203.1302](https://arxiv.org/abs/1203.1302) [hep-ex].
- [15] ATLAS Collaboration, ATLAS-CONF-2011-102.
<https://cdsweb.cern.ch/record/1369219>.

- [16] ATLAS Collaboration, ATLAS-CONF-2012-043.
<https://cdsweb.cern.ch/record/1435197>.
- [17] ATLAS Collaboration, ATLAS-CONF-2012-101.
<https://cdsweb.cern.ch/record/1463915>.
- [18] T. Gleisberg et al., JHEP **0902** (2009) 007, arXiv:0811.4622 [hep-ph].
- [19] J. Alwall et al., JHEP **1106** (2011) 128, arXiv:1106.0522 [hep-ph].
- [20] P. Nason, JHEP **0411** (2004) 040, arXiv:hep-ph/0409146.
- [21] B. P. Kersevan and E. Richter-Was, Comput. Phys. Commun. **149** (2003) 142–194, arXiv:hep-ph/0201302 [hep-ph].
- [22] M. L. Mangano et al., JHEP **0307** (2003) 001, arXiv:hep-ph/0206293.
- [23] J. M. Campbell and R. K. Ellis, Phys. Rev. **D60** (1999) 113006, arXiv:hep-ph/9905386 [hep-ph].
- [24] J. M. Campbell et al., JHEP **1107** (2011) 018, arXiv:1105.0020 [hep-ph].
- [25] F. Campanario et al., Phys. Rev. **D78** (2008) 094012, arXiv:0809.0790 [hep-ph].
- [26] M. Aliev et al., Comput. Phys. Commun. **182** (2011) 1034–1046, arXiv:1007.1327 [hep-ph].
- [27] A. Kardos et al., Phys. Rev. **D85** (2012) 054015, arXiv:1111.0610 [hep-ph].
- [28] J. M. Campbell and R. K. Ellis, JHEP **1207** (2012) 052, arXiv:1204.5678 [hep-ph].
- [29] K. Melnikov and F. Petriello, Phys. Rev. **D74** (2006) 114017, arXiv:hep-ph/0609070 [hep-ph].
- [30] C. Anastasiou et al., Phys. Rev. **D69** (2004) 094008, arXiv:hep-ph/0312266 [hep-ph].
- [31] P. M. Nadolsky et al., Phys. Rev. **D78** (2008) 013004, arXiv:0802.0007 [hep-ph].
- [32] H.-L. Lai et al., Phys. Rev. **D82** (2010) 074024, arXiv:1007.2241 [hep-ph].
- [33] T. Sjöstrand et al., JHEP **0605** (2006) 026, arXiv:hep-ph/0603175.
- [34] J. Butterworth et al., Z. Phys. **C72** (1996) 637–646, arXiv:hep-ph/9601371 [hep-ph].
- [35] GEANT4 Collaboration, S. Agostinelli et al., Nucl.Instrum.Meth. **A506** (2003) 250–303.
- [36] ATLAS Collaboration, Eur. Phys. J. **C 70** (2010) 823–874.
- [37] ATLAS Collaboration, ATL-PHYS-PUB-2010-013.
<https://cdsweb.cern.ch/record/1300517>.
- [38] ATLAS Collaboration, ATLAS-CONF-2010-054.
<https://cdsweb.cern.ch/record/1281311>.
- [39] ATLAS Collaboration, ATLAS-CONF-2011-063. <http://cdsweb.cern.ch/record/1345743>.
- [40] ATLAS Collaboration, ATLAS-CONF-2011-021. <http://cdsweb.cern.ch/record/1336750>.

- [41] ATLAS Collaboration, ATLAS-CONF-2012-097. <https://cdsweb.cern.ch/record/1460443>.
- [42] ATLAS Collaboration, ATLAS-CONF-2011-116. <http://cdsweb.cern.ch/record/1376384>.
- [43] ATLAS Collaboration, Eur. Phys. J. **C 71** (2011) 1630, [arXiv:1101.2185](https://arxiv.org/abs/1101.2185).
- [44] A. L. Read, J. Phys. G **28** no. 10, (2002) 2693.
- [45] G. Cowan et al., Eur. Phys. J. **C 71** (2011) 1–19.
- [46] D0 Collaboration, V. Abazov et al., Phys. Lett. **B638** (2006) 441–449, [arXiv:hep-ex/0605005](https://arxiv.org/abs/hep-ex/0605005) [hep-ex].
- [47] ALEPH Collaboration, A. Heister et al., Eur. Phys. J. **C31** (2003) 1–16, [arXiv:hep-ex/0210014](https://arxiv.org/abs/hep-ex/0210014).
DELPHI Collaboration, J. Abdallah et al., Eur. Phys. J. **C36** (2004) 1–23, [arXiv:hep-ex/0406009](https://arxiv.org/abs/hep-ex/0406009).
L3 Collaboration, P. Achard et al., Phys. Lett. **B524** (2002) 65–80, [arXiv:hep-ex/0110057](https://arxiv.org/abs/hep-ex/0110057).
OPAL Collaboration, G. Abbiendi et al., Eur. Phys. J. **C33** (2004) 149–172, [arXiv:hep-ex/0310054](https://arxiv.org/abs/hep-ex/0310054).
- [48] LEPSUSYWG, ALEPH, DELPHI, L3, OPAL Collaborations, LEPSUSYWG/02-10.1 (2002). http://lepsusy.web.cern.ch/lepsusy/www/rpvlllesummer02/lle_pub.html.
- [49] CMS Collaboration, JHEP **1206** (2012) 169, [arXiv:1204.5341](https://arxiv.org/abs/1204.5341) [hep-ex].
- [50] M. Bahr et al., Eur. Phys. J. **C58** (2008) 639–707, [arXiv:0803.0883](https://arxiv.org/abs/0803.0883) [hep-ph].
- [51] W. Beenakker et al., Nucl. Phys. **B492** (1997) 51–103, [arXiv:hep-ph/9610490](https://arxiv.org/abs/hep-ph/9610490).
- [52] A. Kulesza and L. Motyka, Phys. Rev. Lett. **102** (2009) 111802, [arXiv:0807.2405](https://arxiv.org/abs/0807.2405) [hep-ph].
- [53] A. Kulesza and L. Motyka, Phys. Rev. **D80** (2009) 095004, [arXiv:0905.4749](https://arxiv.org/abs/0905.4749) [hep-ph].
- [54] W. Beenakker et al., JHEP **0912** (2009) 041, [arXiv:0909.4418](https://arxiv.org/abs/0909.4418) [hep-ph].
- [55] W. Beenakker et al., Int. J. Mod. Phys. **A26** (2011) 2637–2664, [arXiv:1105.1110](https://arxiv.org/abs/1105.1110) [hep-ph].
- [56] M. Kramer et al., [arXiv:1206.2892](https://arxiv.org/abs/1206.2892) [hep-ph].